J Fluoresc (2008) 18:715–725
DOI 10.1007/s10895-008-0338-x

ORIGINAL PAPER

Spectroscopic Properties and Conformational Stability of *Concholepas concholepas* Hemocyanin

Krassimira Idakieva · Peter Nikolov · Irena Chakarska · Nicolay Genov · Valery L. Shnyrov

Received: 26 September 2007 / Accepted: 30 January 2008 / Published online: 16 February 2008

Abstract The structure in solution and conformational stability of the hemocyanin from the Chilean gastropod mollusk *Concholepas concholepas* (CCH) and its structural subunits, CCH-A and CCH-B, were studied using fluorescence spectroscopy and differential scanning calorimetry (DSC). The fluorescence properties of the oxygenated and apo-form (copper-deprived) of the didecamer and its subunits were characterized. Besides tryptophan residues buried in the hydrophobic interior of the protein molecule also exposed fluorophores determine the fluorescence emission of the oxy- and apo-forms of the investigated hemocyanins. The copper–dioxygen system at the binuclear active site quenches the tryptophan emission of the oxy-forms of CCH and its subunits. The removal of this system increases the fluorescence quantum yield and causes structural rearrangement of the microenvironment of the emitting tryptophan residues in the respective apo-forms. Time-resolved fluorescence measurements show that the oxygenated and copper-deprived forms of the CCH and its subunits exist in different conformations. The thermal denaturation of the hemocyanin is an irreversible process, under kinetic control. A successive annealing procedure was applied to obtain the experimental deconvolution of the irreversible thermal transitions. Arrhenius equation parameter for the two-state irreversible model of the thermal denaturation of oxy-CCH at pH 7.2 was estimated. Both factors, oligomerization and the copper–dioxygen system at the active site, are important for stabilizing the structure of the hemocyanin molecule.

Keywords Hemocyanin · Molluska · *Concholepas concholepas* · Fluorescence spectroscopy · Differential scanning calorimetry

Abbreviations

Hc	hemocyanin
CCH	*Concholepas concholepas* hemocyanin
DSC	differential scanning calorimetry
EDTA	ethylenediaminetetraacetic acid
MOPS	3-[*N*-morpholino]-propanesulfonic acid
Ac-Trp-NH_2	*N*-acetyltryptophanamide
Tris/HCl	tris (hydroxymethyl) amino-methane hydrochloride

K. Idakieva (✉) · P. Nikolov · I. Chakarska · N. Genov
Institute of Organic Chemistry, Bulgarian Academy of Sciences,
Akad. G. Bonchev-Str. Bl. 9,
Sofia 1113, Bulgaria
e-mail: idakieva@orgchm.bas.bg

V. L. Shnyrov (✉)
Department of Biochemistry and Molecular Biology,
Universidad de Salamanca,
37007 Salamanca, Spain
e-mail: shnyrov@usal.es

Introduction

Hemocyanins (Hcs) are respiratory proteins in many invertebrates, which ensure the circulatory transport of dioxygen to the tissues. The interest in Hcs is due to their important biological function connected with the oxygen

transport and to the possibilities for practical application as immunomodulators.

Native molluskan Hcs are hollow cylinders, approximately 35 nm in diameter [1], and consist of 10 (cephalopodan Hcs) or 20 (gastropodan Hcs) 350–450 kDa subunits. Gastropodan Hcs have didecameric structure, with molecular mass of ~9 MDa and cylinder height of 38 nm [1]. They consist of two axially assembled decamers. The subunits themselves are folded into seven or eight globular substructures, the so-called "functional units" (FUs). Each FU has a molecular mass of approx. 50 kDa and contains one binuclear copper active site, reversibly binding one dioxygen molecule [2, 3].

Under non-physiological conditions Hcs can loose their quaternary structure. The most classical way to obtain dissociation into subunits, without loss of the ability to reversibly bind dioxygen, is an increase of the pH (to ~9) and removal of alkaline-earth cations (by treatment with EDTA) [2, 3]. Gastropodan Hc can also be dissociated under the influence of high pressure (2 kbar) [4]. Data on the conformational stability of Hcs and subunits have been obtained by temperature rise [5, 6] and by treatment with chemical agents like guanidinium chloride and urea [7–9].

Studies on the structure of the Hc from Chilean gastropodan mollusk *Concholepas concholepas* (CCH) have been recently published [10]. This Hc exhibits an unusual heterodecameric array of the two subunits, CCH-A and CCH-B. Moreover, in contrast with other molluskan Hc, its stabilization does not require additional divalent cations in the medium and the re-association of subunits depends on Mg^{2+}[10]. Other specific feature is that the subunit CCH-A has an autocleavage site that under reducing conditions is cleaved to yield two polypeptides, CCH-A1 (300 kDa) and CCH-A2 (108 kDa), whereas CCH-B remains unchanged. It was found that the CCH-A nick is not inhibited by the addition of protease inhibitors and/or divalent cations [10]. CCH has been successfully used as a carrier in the antibody development [11]. Recently, it has been reported that this protein is effective for preventing tumor growth in a murine bladder cancer model like widely used keyhole limpet hemocyanin (KLH) [12].

The present study was performed in order to obtain new data about the structure in solution and the conformational stability of the Chilean gastropod *Concholepas concholepas* hemocyanin and the structural subunits constituting the Hc molecule. The influence of dissociation and of removal of copper was also investigated.

Materials and methods

Hemocyanin

Concholepas concholepas hemocyanin was purchased from Biosonda Corp., Chile. To dissociate CCH into its subunits, the protein samples were dialyzed overnight against 130 mM Glycine/NaOH buffer, pH 9.6, containing 10 mM EDTA. The two structural subunits CCH-A and CCH-B were purified by FPLC, using Mono-Q HR 10/10 anion-exchange column (Amersham Biosciences, Uppsala, Sweden), as described in [10].

The apo-forms (copper-deprived) of CCH and isolated subunits, CCH-A and CCH-B, were prepared by dialysis against 50 mM Tris/HCl, containing 25 mM KCN, pH 7.2, for 48 h, at 4 °C, according to [13]. The samples were then dialyzed against 50 mM Tris/HCl, containing 10 mM EDTA at pH 7.2, and finally against 50 mM Tris/HCl, pH 7.2.

Spectroscopic methods

UV-VIS absorption spectrophotometry

Absorption spectra were recorded with a spectrophotometer Shimadzu model 3000. Protein concentration was determined spectrophotometrically using the absorption coefficient $A_{278}^{0.1\%} = 1.36\ \mathrm{mg^{-1}\ ml\ cm^{-1}}$.

Steady-state fluorescence measurements

Fluorescence measurements were carried out on a Perkin Elmer model LS 5 spectrofluorimeter equipped with a thermostatic cell compartment and a Data Station model 3600. The position of a chord drawn at the 80% level of maximum intensity was taken as the position of the spectrum. The optical density of the solutions was lower than 0.05 at the excitation wavelength to avoid inner filter effects. The relative quantum yields were measured by comparing the integrated corrected fluorescence spectra of Hcs with those of *N*-acetyltryptophanamide (Ac-Trp-NH_2), normalized to the same absorbance at the excitation wavelength. The quantum yield of the standard was 0.13 at 21 °C [14].

The results of the quenching reactions between the excited tryptophan side chains and acrylamide or KI were analyzed according to the Stern–Volmer equation [15]:

$$F_0/F = 1 + K_Q[Q] \tag{1}$$

where F_0 and F are the fluorescence intensities in the absence and in the presence of quencher, respectively; K_Q is the collisional quenching constant and $[Q]$ is the quencher concentration. A small amount of $Na_2S_2O_3$ was added to the iodide solutions to prevent I_3^- formation. The inner filter effect due to the acrylamide was corrected by the factor:

$$Y = \mathrm{antilog}(d_A + d_B)/2 \tag{2}$$

where d_A and d_B are the optical densities at the excitation and emission wavelength, respectively. Static quenching with

acrylamide was separated from the total effect by the equation [16]:

$$F_0 \Big/ F.e^{-V[Q]} = 1 + K_Q[Q] \quad (3)$$

where V is the static quenching constant which is related to the probability of finding a quencher molecule close enough to the chromophore at the moment of excitation, to quench it statically.

Since in multitryptophan proteins, with a heterogeneous distribution of fluorescing groups, each fluorophor may have different quenching constants, the measured decrease in fluorescence emission can be a non linear function of the concentration of the quenching agent. In this case, the quenching effect is better described by a modified Stern–Volmer equation:

$$F_0/(F_0 - F) = (1/[Q])\left(1/\Sigma f_i K_{Qi}\right) + \Sigma K_{Qi}/\Sigma f_i K_{Qi} \quad (4)$$

where F_0, F and $[Q]$ are as defined above, and f_i and K_{Qi} represent, respectively, the fractional fluorescence and the quenching constant relative to the i-th tryptophan residue. Plotting $F_0/(F_0 - F)$ vs $1/[Q]$, the ratio intercept/slope express $\Sigma K_{Qi} = \left(K_Q\right)_{\text{eff}}$, the effective quenching constant, and 1/intercept express $\Sigma f_i K_{Qi}/\Sigma K_{Qi} = (f_a)_{\text{eff}}$, the effective fraction of fluorescence accessible to the quencher [15].

Time-resolved fluorescence measurements

Time-resolved fluorescence studies were performed at 20 °C using a nanosecond single-photon-counting spectrofluorimeter (system PRA 2000) and a nitrogen-filled flash lamp with a full width at half-maximum of ~2.5 ns. The protein samples were dissolved in 50 mM Tris/HCl buffer, pH 7.2. For measurements of the subunits 50 mM Tris/HCl buffer, containing 10 mM EDTA, pH 9.0, was used. The data were analyzed by convoluting the instrument response function $L(t')$ with an assumed decay function $P(t)$, as

$$Y_c(t) = \int_0^t L(t')P(t - t')dt' \quad (6)$$

and comparing Y_c (t) with the experimental time-dependence $R_m(t)$ using a nonlinear least-squares iterative convolution method based on the Marquardt algorithm. The decay curves contained 10^4 counts at the maxima and the time-resolution for these curves was 100 ps per channel. The goodness of the fit was assessed by the weighted residuals and the reduced χ^2-test.

Differential scanning calorimetry

Calorimetric measurements were performed on a high-sensitivity differential scanning microcalorimeter DASM-4 (Biopribor, Pushchino, Russia), with sensitivity greater than 0.017 mJ/K and a noise level less than ±0.05 μW. Different scan rates within the 0.5–2 K min^{-1} range were employed. A constant pressure of 2 atm was maintained during all DSC experiments to prevent possible degassing of the solution on heating. Before measurements the protein samples were dialyzed extensively against buffer 20 mM MOPS, pH 7.2 (20 °C). The reversibility of the thermal transitions was checked by examining the reproducibility of the calorimetric trace in a second heating of the sample immediately after cooling from the first scan. In all cases, the thermal denaturation was found to be irreversible, therefore the thermogram corresponding to the reheating run was used as instrumental base line. The transitions were corrected for the difference in heat capacity between the initial and final state by using the chemical base line, in accordance with [18]. The molar excess heat capacity curves, obtained by normalizing with the protein concentrations and the known volume of the calorimetric cell, were smoothed and plotted using the Windows-based software package (Origin) supplied by MicroCal. The data were analyzed by non-linear least-squares fitting programs, as reported elsewhere [19]. In all cases the correlation coefficient (r), used as a criterion for the accuracy of fitting was calculated according to the equation:

$$r = \sqrt{1 - \sum_{i=1}^{n}\left(y_i - y_i^{\text{calc}}\right)^2 \Big/ \sum_{i=1}^{N}\left(y_i - y_i^{\text{m}}\right)^2} \quad (7)$$

where y_i and y_i^{calc} are, respectively, the experimental and calculated values of the measurable parameter; y_i^{m} is the mean of the experimental values of the measurable parameter and n the number of points. In the calculation of molar quantities the molecular mass used for the protein was 9,000 kDa.

Results and discussion

Steady-state fluorescence measurements

Steady-state fluorescence parameters of the oxy- and apo-forms of the CCH and its structural subunits, CCH-A and CCH-B, are summarized in Table 1. After excitation at 280 nm, where is the main absorption maximum of the tyrosine and tryptophan residues, or at 295 nm, where the tryptophan side chains are selectively excited, the fluorescence spectra of the oxy-forms of CCH and its subunits, CCH-A and CCH-B, have maxima at 335±1, 338±1 and 343±1 nm, respectively. Red shift in the tryptophan fluorescence spectra positions to 344±1, 346±1 and 346±1 nm was observed for the respective apo-Hcs, indicating

Table 1 Steady-state fluorescence parameters of CCH and its subunits CCH-A and CCH-B

Protein	Emission λ_{max} (nm) (excitation at 295 nm)	Relative quantum yield	Acrylamide quenching		KI quenching	
			K_Q (M^{-1})	V (M^{-1})	K_Q (M^{-1})	f_a
oxy-CCH	335±1	0.02	0.65	–	–	–
oxy-CCH-A	338±1	0.02	1.22	–	–	–
oxy-CCH-B	343±1	0.03	1.79	–	–	–
apo-CCH	344±1	0.1	2.85	–	9.19	0.42
apo-CCH-A	346±1	0.1	3.01	–	1.66	–
apo-CCH-B	346±1	0.1	3.19	0.6	10.8	0.37
Ac-Trp-NH_2	350±1	0.130[a]	16.33[a]	2.0	11.70[a]	1.00

[a] Data from [30]

that removal of the copper atoms at the active sites and dissociation into subunits of the copper-deprived Hc change the microenvironment of the emitting tryptophan residues.

In addition to the wavelength shifts, pronounced differences in the quantum yields, already reported in other Hcs [7, 8] were observed. While the tryptophan emission quantum yield of the oxy-forms of CCH and its subunits is low (0.02–0.03; Table 1), a quantum yield of 0.1 has been determined for the respective apo-forms. The observed effect can be explained by radiationless energy transfer from the excited indole rings to the copper–dioxygen system in the oxy-form. Recently, Erker et al. [21] presented a detailed study, at atomic level resolution, that Förster transfer is responsible for the oxygen-dependent quenching of the tryptophan fluorescence in tarantula (arthropod) Hc. The tryptophans transfer their excitation energy to the oxygenated active sites.

The absence of tyrosine emission in the fluorescence spectra of the investigated Hcs after excitation at 280 nm can be explained by a singlet–singlet radiationless energy transfer from phenol groups (donors) to indole rings (acceptors) according to Förster's theory of electronic energy transfer in donor–acceptor systems [22]. Similar explanation has been given at the fluorescence measurements of the Hc of the related gastropods *Rapana thomasiana* (RtH) and β-Hc of *Helix pomatia* (β-HpH) [23, 24].

According to the model of discrete states of tryptophan residues in proteins there are several most probable physical states for the emitting fluorophores [25, 26]. Each state is characterized by its fluorescence spectrum. Analysis of the emission spectra of CCH and its subunits (Fig. 1) on the basis of this model shows that they can be fitted by four spectral components, two of which (forms S and I) are due to the emission of buried tryptophans in a polar environment (spectral form S corresponds to the emission of the indole chromophore located inside the protein and forming a 1:1 exciplexes with some neighbouring polar protein group, while spectral form I corresponds to the emission of

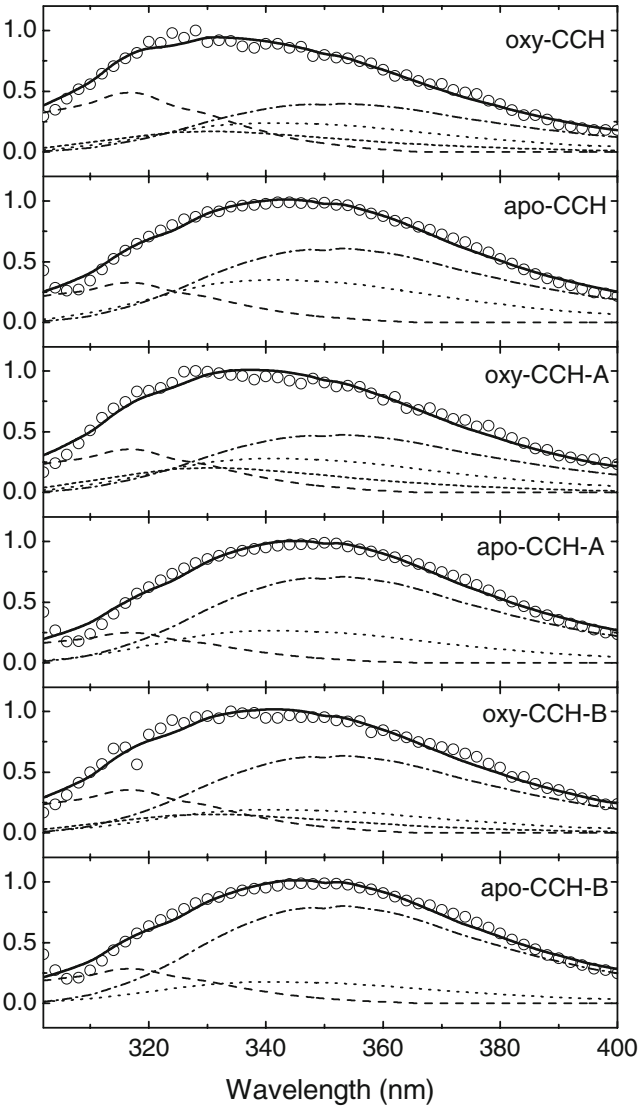

Fig. 1 Fitting of the experimental fluorescence spectra data (*symbols*) of the oxy- and apo-forms of CCH, CCH-A and CCH-B to the theoretical model of discrete states of tryptophan residues in proteins [25] (*continues lines*), which are sums of the following spectral components: S (*dashed line*); I (*short-dashed line*); II (*dotted line*); III (*dash-dotted line*)

Table 2 Contribution to the fluorescence emission of CCH and its subunits, CCH-A and CCH-B, of spectral forms (%), according to the model of discrete states of tryptophan residues in proteins [25]

Protein	Spectral forms (%)			
	S	I	II	III
oxy-CCH	26.5	13.3	21.6	38.6
apo-CCH	16.6	0	30.1	53.3
oxy-CCH-A	18.0	15.0	23.9	43.1
apo-CCH-A	13.4	0	22.7	63.9
oxy-CCH-B	17.4	10.9	15.8	55.9
apo-CCH-B	15.2	0	15.9	68.9

chromophore forming a 2:1 exciplexes in the same environment). The other (form II and form III) are due to the emission of tryptophans located at the protein surface (spectral form II corresponds to the emission of the chromophore which is in contact with bound water, while spectral form III corresponds to the emission of the chromophore which is in contact with free water molecules). In Table 2 the estimated contribution to the emission of investigated Hcs of the spectral forms, corresponding to the model of discrete states of tryptophan residues in proteins, is shown. Besides buried tryptophans the fluorescence of oxy-CCH is determined also by fluorophores in contact with free water. In the spectra of the subunits CCH-A and especially CCH-B, exposed tryptophan residues provide considerable contribution to the fluorescence emission. Conformational changes in the proteins after copper removal change the polarity of the environment of the buried tryptophan residues (forms S and I).

Inspection of the crystallographic structure of FU RtH2-*e* isolated from the Hc of *Rapana thomasiana* [27] shows that Trp-69, which is completely conserved in molluscan Hcs, is in the immediate microenvironment of the dioxygen-binding site, at a distance of 5–6 Å from the copper atom Cu_A. Hence, its emission should be very sensitive to conformational changes in the region of the active site. The other indole groups are located at a distance of ≥10 Å from this site and are buried in the hydrophobic interior of the globule. Results from the analysis of the emission spectra of CCH and its subunits show considerable presence of exposed fluorophores, which is a different feature of this Hc. By means of surface-enhanced Raman spectroscopy has been shown the relative abundance of the amino acids tryptophan and cystine in the molecule of CCH in comparison with KLH [28].

Acrylamide- and I-fluorescence quenching studies

Acrylamide is an efficient neutral quencher of tryptophan fluorescence and provides topographical information about the emitting chromophores [16]. It can discriminate between "exposed" and "buried" tryptophan side chains and the results are not influenced by the charge of the chromophore microenvironment. The ability to quench collisionally the excited indole rings depends on its ability to penetrate the protein matrix. Quenching of "buried" tryptophans by acrylamide has been explained in terms of structural fluctuations of the protein molecules that facilitate the inward diffusion of the quencher [25]. The fluorescence quenching with acrylamide of the oxy-forms of CCH and the subunits, CCH-A and CCH-B, followed the classical Stern–Volmer Eq. 1 (Fig. 2). The observed linearity of the Stern–Volmer plot can be explained by the similarity of the individual K_Q constants of the tryptophan fluorophors [29]. This means that tryptophan residues of the protein differ only slightly in accessibility, although discrimination among the indole fluorophores could be expected as CCH is multitryptophan protein. Similar linear plots have also been observed during the investigation on the oxy-forms of RtH, β-HpH and their subunits [23, 24]. The slope of the plots at a low concentration of acrylamide reflects to a large extent the quenching of the more accessible residues and selective quenching can be observed only if the K_Q constants differ sufficiently [26]. K_Q values of 0.65, 1.22 and 1.79 M^{-1} were calculated for the CCH, CCH-A and CCH-B, respectively (Table 1). These constants are significantly lower than the value for Ac-Trp-NH_2, i.e. for tryptophan in aqueous solution, and reflect the additional limitations of the accessibility of the quencher molecules to the emitting tryptophans imposed by the quaternary structure of the aggregates.

With apo-CCH and apo-CCH-A the values of K_Q, 2.85 and 3.01 M^{-1} respectively, are significantly higher than

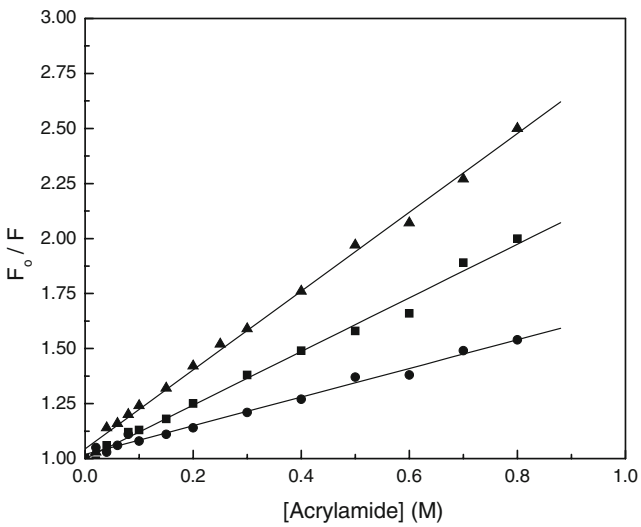

Fig. 2 Stern–Volmer plots for the quenching of the fluorescence of the oxy-forms of CCH (*circle*) and its subunits CCH-A (*square*) and CCH-B (*triangle*) by acrylamide, according to Eq. 1. The experiments were performed at 25 °C after excitation of the protein samples at 295 nm

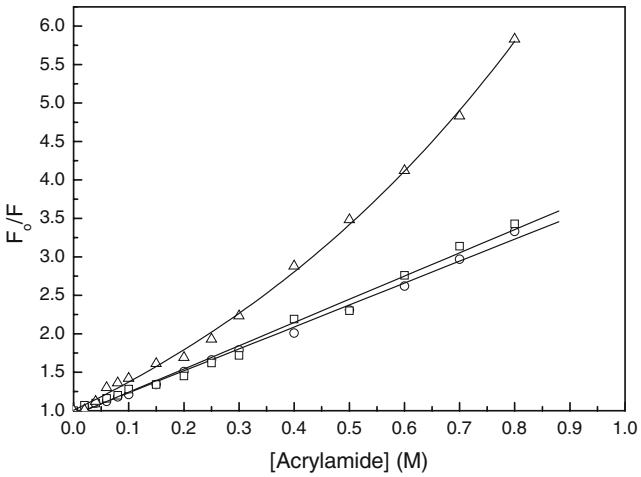

Fig. 3 Stern–Volmer plots for the quenching of the fluorescence of the apo-forms of CCH (*circle*), CCH-A (*square*) and CCH-B (*triangle*) by acrylamide, according to Eq. 1

those for the oxy-forms (Table 1). The Stern–Volmer plot for the apo-form of CCH-B tryptophan fluorescence quenching with acrylamide showed upward curvature (Fig. 3). In this case the fluorescence of all tryptophan residues is equally quenched (nearly equally accessible chromophores), or only part of them are fluorescent [16]. The best fit of the curve to the linear plot was obtained using the modified Stern–Volmer relationship of Eq. 3 and a value of 0.6 M^{-1} for the static quenching constant. The parameter V is related to the probability of finding the quencher molecule close enough to the excited chromophore to quench it with 100% efficiency. A value of V= 2.0 M^{-1} has been obtained for the quenching of the Ac-Trp-NH_2 fluorescence by acrylamide [16]. The value calculated for the apo-form of CCH-B thus indicates that the local concentration of acrylamide molecules in the proximity of the emitting tryptophans is moderate. It thus can be concluded that the tryptophan residues in the apo-forms of the CCH and its subunits become more exposed than in the oxy-Hcs. The removal of the copper at the binuclear active sites causes a structural rearrangement of the microenvironment of the emitting tryptophan residues and they are more accessible to the quencher molecules than in the respective oxygenated form of the proteins.

Quenching experiments were also performed with ionic quencher KI. Ionic quenchers, like I^-, are charged and hydrated. In contrast with acrylamide, which can penetrate the protein matrix, they are able to quench only surface fluorophores and are effective in discriminating between "exposed" and "buried" chromophores, as well as in revealing charge effects. Exposure of the oxy-forms of CCH and its subunits to increasing I^- concentrations [0.02–0.8 M] had no effect on their fluorescence after excitation at 295 nm. The low quenching efficiency of I^- can be explained by electrostatic repulsion due to the negative charge of the microenvironment of emitting tryptophans. After copper removal the apo-forms of the studied Hc molecules become more accessible to the ionic quencher I^-. K_Q values of 1.66 M^{-1} was calculated for the subunit CCH-A (Table 1). On the other hand, I^- quenching plots for CCH and the subunit CCH-B demonstrate heterogeneity of the tryptophan emission, as shown by the considerable downward curvature of the plots (Fig. 4). The modified Stern–Volmer plots, then, allow us evaluating the fraction and the K_Q value of the most quencher-accessible fluorescence (Table 1). As can be seen in apo-CCH and apo-CCH-B, 37–42% of the total fluorescence emission is accessible to the quenching action of I^- ions. Quenching experiments reveal differences between Trp environments in the structural subunits CCH-A and CCH-B. The observed increase in the quenching efficiency on the tryptophan emission of the CCH subunits can be explained by assuming that upon dissociation, tryptophan side chains, located in the protein inter-subunit contact area, become more accessible to the quencher.

Effect of pH on the conformational stability

The effect of pH on the tryptophan fluorescence quantum yield of the oxy-forms of the CCH and its subunits, CCH-A and CCH-B, is shown in Fig. 5. Practically no change in the emission of oxy-CCH and oxy-CCH-A was observed in the pH region 5.0–8.0. In the case of subunit CCH-B the region of stability is between pH 6.0 and 8.0. Increase of the fluorescence quantum yield at pH values above 8 can be attributed to the titration of an ionizable group with apparent pK_a of 8.1, which is within the ionization region

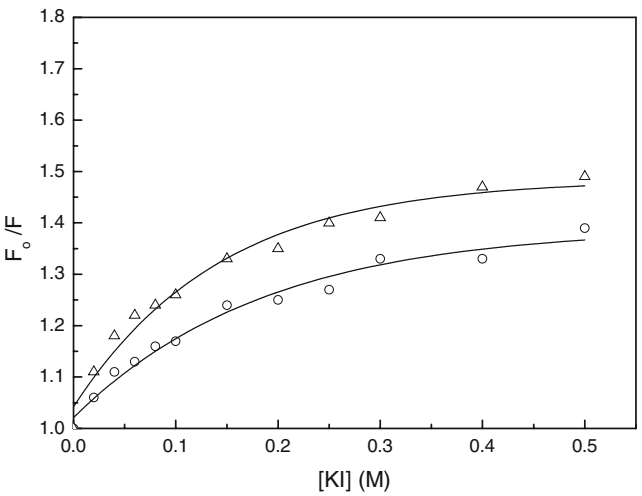

Fig. 4 Stern–Volmer plots for the quenching of the fluorescence of the apo-forms of CCH (*circle*) and CCH-B (*triangle*) by KI, according to Eq. 1

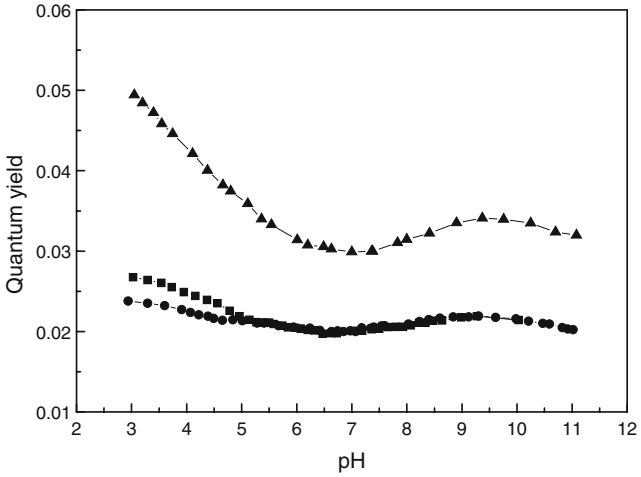

Fig. 5 pH-dependence of the tryptophan fluorescence quantum yield of the oxy-forms of CCH (*circle*) and its subunits CCH-A (*square*) and CCH-B (*triangle*). The following buffers were used: 50 mM sodium citrate (pH 3.0–7.0); 50 mM Tris/HCl (pH 7.0–9.0); 50 mM carbonate/bicarbonate (pH 9.0–11.0)

of the α-amino group. Alternatively, the quenching process may involve electron transfer from an excited tryptopan residue to the α-amino group or to an ε-amino group with abnormal pK, which can occur over an appreciable distance. The transition with a midpoint at pH 6.0 most probably represents the apparent pK_a of imidazole groups of histidyl residues. The emission of tryptophan residues in the apo-Hcs is thus most likely quenched by nearby protonated imidazole groups, which are able to form complexes with indole (Fig. 6). The transition at pH≈10.5, also observed for the oxy-forms, can be ascribed to ionization of tyrosine residues and efficient radiationless energy transfer from the excited indole rings to ionized phenol groups. The small increase of the fluorescence quantum yield of the oxy-forms below pH 5.0 is probably a result of a destruction of the copper–dioxygen system at the active site, which quenches the tryptophan fluorescence. There is not such a system in the apo-form of the Hcs and for this reason no increase of the fluorescence quantum yield is observed in this case.

Time-resolved fluorescence measurements

For the further characterization of the conformational states of oxy- and apo-forms of CCH and its structural subunits, CCH-A and CCH-B, we used time-resolved fluorescence spectroscopy. This method provides information about the molecular environment of the fluorophores. The fluorescence decay of the Hcs was investigated upon excitation at 297 nm, where the light is selectively absorbed by the tryptophan chromophores, and was fitted by bi-exponential decay function. The theoretical fluorescence intensity at time t is given by the function $I^F(t) = A_1 . \exp(-t/\tau_1) + A_2 . \exp(-t/\tau_2)$, where A_1 and A_2 are amplitudes. The value of the parameter χ^2 was around 1.2 (Table 3); the residuals between the theoretical and experimental decay curves as well as autocorrelation plots were flat and random, which demonstrates a good quality of the fit. Figure 7 shows the fluorescence decay of oxy CCH-A. The calculated lifetimes, the relative amplitudes and the χ^2-values are shown in Table 3. The comparison of the data for the oxy-forms of CCH and its subunits shows some differences in the shorter lifetime, τ_1. While for CCH and CCH-A the shorter lifetimes are similar—0.38 and 0.34 ns, respectively, the structural subunit CCH-B has lower τ_1-value of 0.28 ns. The apo-forms of CCH and its subunits have practically the same shorter lifetimes—0.24–0.26 ns, but lower than those for the respective oxy-forms (Table 3). The differences were also observed for the longer lifetime components τ_2: 2.34 and 2.52 ns for the oxy-CCH and oxy-CCH-A compare with the τ_2-value of 2.06 ns for oxy-CCH-B. For the respective apo-forms of the Hcs the longer lifetime components τ_2 are between 2.61 and 3.11 ns (Table 3). These results also show some changes in the microenvironment of the tryptophan chromophores between the oxy-forms of the CCH and the subunit CCH-A compare with the subunit CCH-B. However, no significant differences were observed between the apo-forms of the investigated Hcs. On the other hand the parameters obtained from the analysis of the fluorescence decay curves (Table 3) demonstrate conformational changes in the native CCH and its subunits upon the transition from oxy- to the apo-forms. These results are in agreement with the conclusions made on the basis of the steady-state fluorescence measurements. Dynamic light scattering and time-resolved fluorescence measurements of the *Rapana thomasiana* Hc and its substructures also showed that the proteins adopt different conformations in their native, oxidized or copper-deprived form [31].

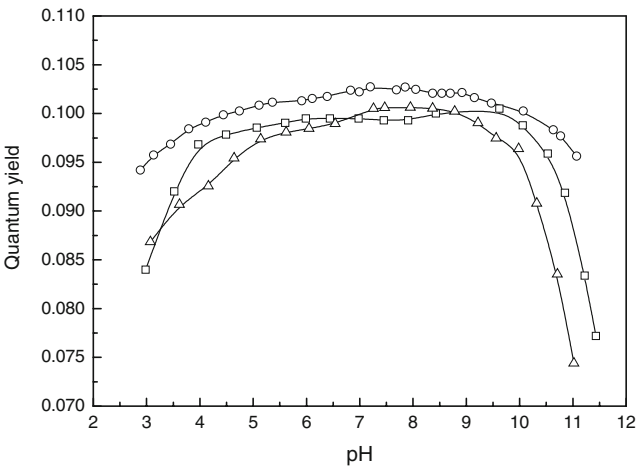

Fig. 6 pH-dependence of the tryptophan fluorescence quantum yield of the apo-forms of CCH (*circle*), CCH-A (*square*) and CCH-B (*triangle*). The buffers used are as described for Fig. 5

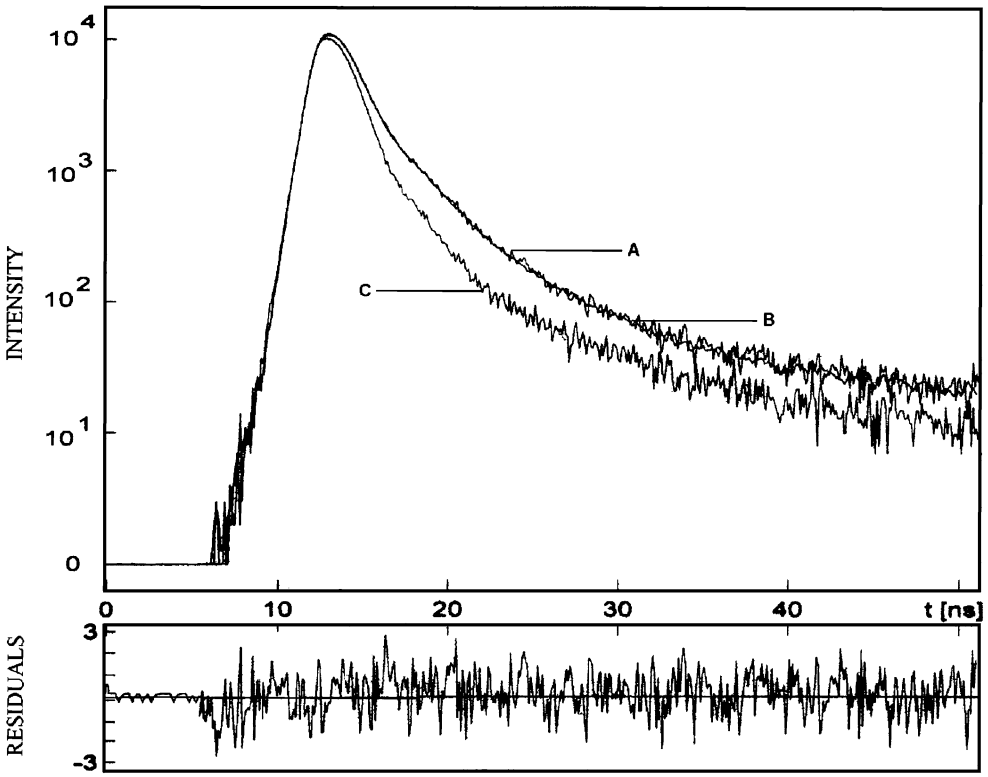

Fig. 7 Fluorescence decay of the oxy-form of subunit CCH-A in 50 mM Tris/HCl buffer, pH 7.2, λex=297 nm, λem=350 nm. *Curve A* Experimental data for the fluorescence decay; *curve B* convoluted results with bi-exponential decay function; *curve C* instrumental response function

Thermostability measurements

The thermal stability of the oxy-form of CCH was studied by high-sensitivity differential scanning calorimetry. The thermal denaturation of the Hc in buffer 50 mM MOPS, pH 7.2, at a scanning rate of 1 K/min, was irreversible judging from the absence of any transitions upon rescanning the samples. Irreversibility of the thermal denaturation was observed also in the DSC measurements of the Hcs from *Rapana thomasiana* [6], *Helix pomatia* [24, 32], lobster *Palinurus vulgaris* [5] and tarantula *Eurypelma californicum* [33] and is a common property of the large hemocyanin molecules.

Since CCH is an oligomeric protein, thermally induced denaturation could be accompanied by dissociation into subunits. The T_m and ΔH_{cal} values for the thermal denaturation of CCH were found to be independent of the protein concentration within the 2.0–6.5 mg/ml range (data not shown). For the irreversible transition luck of dependence of melting temperature on the protein concentration indicates that the dissociation of the monomers is not part of the rate determining irreversible reaction.

Table 3 Fluorescence decay parameters of CCH and its subunits CCH-A and CCH-B after excitation at 297 nm

Protein	τ_1 (ns)	A_1 (%)	τ_2 (ns)	A_2 (%)	χ^2
oxy-CCH	0.38	75	2.34	25	1.23
oxy-CCH-A	0.34	66	2.52	34	1.19
oxy- CCH-B	0.28	61	2.06	39	1.23
apo-CCH	0.25	57	2.93	43	1.18
apo-CCH-A	0.24	53	2.61	47	1.20
apo-CCH-B	0.26	60	3.11	40	1.24

Owing to the irreversibility of the thermal denaturation of CCH thermodynamic parameters cannot be obtained because of the strong distortion of the DSC transitions due to the kinetics of the irreversible formation of the final state. Nevertheless, it is possible to obtain kinetic information from the analysis of the irreversible process. Figure 8 shows the corrected calorimetric traces i.e., the excess specific heat capacity function vs temperature profiles for oxy-CCH in buffer 50 mM MOPS, pH 7.2, at three different scan rates (0.5, 1.0 and 2.0 K/min). The transition temperature of the irreversible thermal denaturation of CCH is dependent on the scan rate: the maximum of the DSC profiles is shifted toward lower temperatures with a decrease in the heating rate, indicating that the process is kinetically controlled.

We apply a successive annealing procedure, which is useful for the experimental deconvolution of complicated completely or partially irreversible thermal transitions, for analysis of the DSC contours [32, 34–36]. Figure 8 shows the final results of this procedure (dashed and continuous lines), which provides three irreversible transitions.

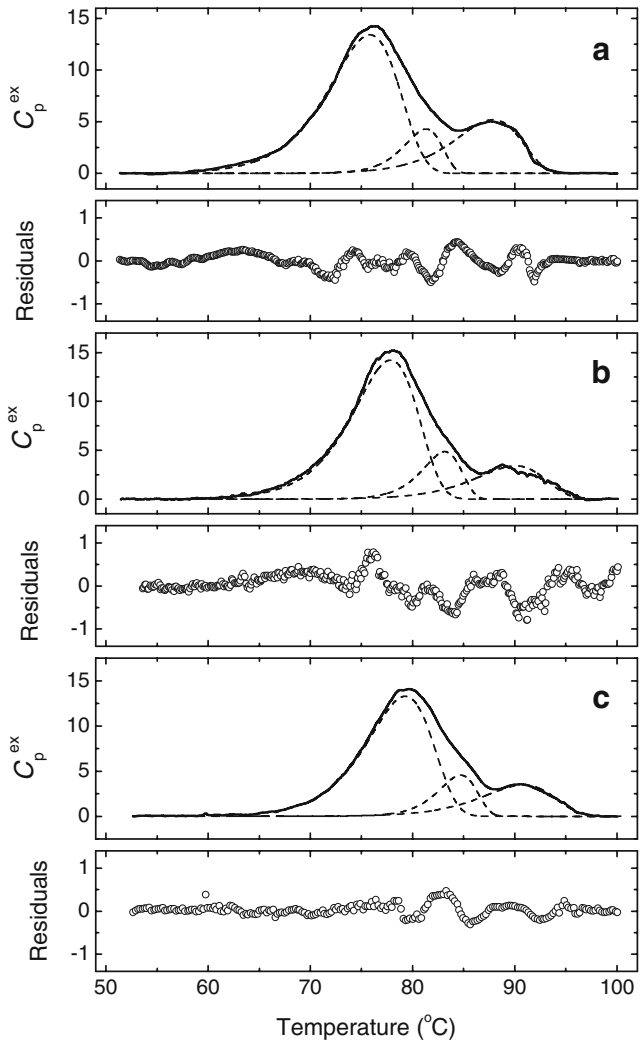

Fig. 8 Temperature dependence of the excess heat capacity of oxy-CCH at scan rates of 0.5 (**a**), 1.0 (**b**) and 2.0 K·min^{-1} (**c**) with corresponding residuals shown in the bottom panels. *Continuous lines* show the experimental data and *dashed lines* are result of the experimental deconvolution of the heat capacity curves into individual components with the successive annealing procedure

DSC traces for the CCH were strongly dependent on the scan rate, which prompted us to analyse this non-equilibrium process based on the simplest so-called two-state kinetic model:

$$N \xrightarrow{k} D \tag{8}$$

which is a limiting case of the Lumry–Eyring model [37]. This model considers only two significantly populated macroscopic states: the initial or native state (N), and the final or denatured state (D), the transition between which is determined by a strongly temperature-dependent first-order rate constant (k). In this case, the excess heat capacity C_p^{ex} is given by the following equation [19]:

$$C_p^{ex} = \frac{1}{v}\Delta H \exp\left\{\frac{E_A}{R}\left(\frac{1}{T^*}-\frac{1}{T}\right)\right\} \times \exp\left\{-\frac{1}{v}\int_{T_0}^{T}\exp\left[\frac{E_A}{R}\left(\frac{1}{T^*}-\frac{1}{T}\right)\right]dT\right\} \tag{9}$$

where $v = dT/dt(K/min)$ is a scan rate value, ΔH is the enthalpy difference between the denatured and native states, E_A is the activation energy of the denaturation process, R is a gas constant, and T^* is the temperature, where k is equal to 1 min^{-1}. The kinetic parameters obtained from the fitting the experimental data to the two-state irreversible model (Eq. 9) are presented in Table 4.

In view of the complex oligomeric Hc structure, the presence of more than one structural domains undergoing thermal unfolding more or less independently of each other is not unexpected. It was mentioned that the splitting of the subunit CCH-A might be similar to that previously described for the subunit RtH2 of *Rapana* hemocyanin [10, 38]. In fact, *Concholepas* and *Rapana* are closely related neogastropods (*Muricidae* and *Rapaninae*). The existence of

Table 4 Arrhenius equation parameter estimates for the two-state irreversible model of the thermal denaturation of oxy-CCH at pH 7.2

Transition	Parameter	Temperature scan rate (K min^{-1})			
		0.5	1.0	2.0	Global fitting
First	ΔH (MJ mol^{-1})	122±1	120±1	113±1	
	T^* (°C)	82.5±0.1	81.6±0.1	80.8±0.2	81.5±0.2
	E_A (kJ mol^{-1})	296±2	323±2	323±3	324±3
	r	0.9982	0.9912	0.9989	0.9957
Second	ΔH (MJ mol^{-1})	21±1	24±1	23±1	
	T^* (°C)	83.8±0.2	84.4±0.2	84.6±0.2	84.5±0.2
	E_A (kJ mol^{-1})	566±6	563±5	572±8	567±6
	r	0.9913	0.9903	0.9893	0.9902
Third	ΔH (MJ mol^{-1})	44±1	31±1	32±1	
	T^* (°C)	94.1±0.2	94.3±0.3	92.8±0.1	94.2±0.2
	E_A (kJ mol^{-1})	334±5	322±5	317±4	320±5
	r	0.9941	0.9892	0.9906	0.9900

an inter-FU disulfide bridge located between FU *f* from the wall and FU *g* from the collar of the cylindrical Hc molecule of RtH is a hypothetical reason that can be invoked to account for the two transitions seen in the thermogram [6]. The observed nick also should make the molecule of CCH more unstable. Actually, compared to the β-HpH, the thermograms of CCH and RtH have a more complex character [6, 24, 32].

The apo-form of CCH showed lower thermostability compared to the respective oxy-form. The T_m value of the main transition is at 57.4 °C, which is ~20° lower than the T_m obtained for the oxy-CCH (data not shown). This result, similarly to data obtained for apo-β-HpH [24] demonstrates the contribution of the copper–dioxygen system at the binuclear active sites to the stability of the Hc structure. Study of nine Hcs from arthropod and gastropod organisms by circular dichroism also has shown that the hemocyanin thermostability is highly dependent on the presence or absence of the copper-containing dioxygen-binding sites [39].

In conclusion, the present investigations allow physico-chemical characterization of the CCH and the constituent structural subunits. Besides tryptophan residues buried in the hydrophobic interior of the protein molecule also exposed fluorophores determine the fluorescence emission of the oxy and apo-forms of the investigated Hc. The oxygenated and copper-deprived forms of the CCH and its subunits exist in different conformations. Both factors, oligomerization and the copper–dioxygen system at the active site, are important for stabilizing the structure of the hemocyanin molecule.

Acknowledgements This work was supported by research grant TK-X-1611 from the NSF of the Ministry of Education and Science, Bulgaria.

References

1. van Bruggen EFJ, Schutter WG, van Breemen JFL, Bijlholt MMC, Wichertjes T (1981) In: Harris JR (ed) Electron microscopy of proteins, vol. I. Academic, London, New York, pp 1–38
2. Préaux G, Gielens C (1984) In: Lontie R (ed) Copper proteins and copper enzymes, vol. II. CRC, Boca Raton, FL, pp 159–205
3. van Holde KE, Miller KI (1995) Hemocyanins. Adv Prot Chem 47:1–81
4. Bonafe CFS, Araujo JV, Silva JL (1994) Intermediate states of assembly in the dissociation of gastropod hemocyanin by hydrostatic pressure. Biochemistry 33:2651–2660
5. Guzman-Casado M, Parody-Morreale A, Mateo PL, Sanchez-Ruiz JM (1990) Differential scanning calorimetry of lobster hemocyanin. Eur J Biochem 188:181–185
6. Idakieva K, Parvanova K, Todinova S (2005) Differential scanning calorimetry of the irreversible denaturation of *Rapana thomasiana* (marine snail, Gastropod) hemocyanin. Biochim Biophys Acta 1748:50–56
7. Hübler R, Fertl B, Hellmann N, Decker H (1998) On the stability of the 24-meric hemocyanin from *Eurypelma californicum*. Biochim Biophys Acta 1383:327–339
8. Favilla R, Goldoni M, Mazzini A, Di Muro P, Salvato B, Beltramini M (2002) Guanidinium chloride induced unfolding of a hemocyanin subunit from *Carcinus* aestuarii. I. Apo form. Biochim Biophys Acta 1597:42–50
9. Favilla R, Goldoni M, Mazzini A, Del Signore F, Di Muro P, Salvato B, Beltramini M (2002) Guanidinium chloride induced unfolding of a hemocyanin subunit from *Carcinus aestuarii*. II. Holo form. Biochim Biophys Acta 1597:51–59
10. De Ioannes P, Moltedo B, Oliva H, Pacheco R, Faunes F, De Ioannes AE, Becker MI (2004) Hemocyanin of the molluscan *Concholepas concholepas* exhibits an unusual heterodecameric array of subunits. J Biol Chem 279:26134–26142
11. Manoslava H, De Ioannes AE, Becker M I (2004) Development of monoclonal antibodies bearing the internal image of the gizzerosine epitope and application in a competitive ELISA for fish meal. Hybridoma Hybridomics 23:45–54
12. Moltedo B, Faunes F, Haussmann D, de Ioannes P, De Ioannes AE, Puente J, Becker M I (2006) Immunotherapeutic effect of *Concholepas* hemocyanin in the murine bladder cancer model: evidence for conserved antitumor properties among hemocyanins. J Urol 176:2690–2695
13. Beltramini M, Ricchelli F, Salvato B (1984) The kinetics of the reaction of *Octopus vulgaris* hemocyanin with cyanide. Its significance for the structure of the 11S subunit of molluscan hemocyanin. Inorg Chim Acta 92:209–217
14. Kirby EP, Steiner RF (1970) The tryptophan microenvironment in apo-myoglobin. J Biol Chem 245:6300–6306
15. Lehrer SS (1971) Solute perturbation of protein fluorescence. The quenching of the tryptophyl fluorescence of model compounds and of lysozyme by iodide ion. Biochemistry 10:3254–3263
16. Eftink MR, Ghiron CA (1976) Exposure of tryptophyl residues in proteins. Quantitative determination by fluorescence quenching studies. Biochemistry 15:672–680
17. Kirby EP, Steiner RF (1970) The influence of solvent and temperature upon the fluorescence of indole derivatives. J Phys Chem 74:4480–4490
18. Takahashi K, Sturtevant JM (1981) Thermal denaturation of Streptomyces subtilisin inhibitor, subtilisin BPN', and the inhibitor–subtilisin complex. Biochemistry 20:6185–6190
19. Kurganov BI, Lyubarev AE, Sanchez-Ruiz JM, Shnyrov VL (1997) Analysis of differential scanning calorimetry data for proteins, criteria of validity of one-step mechanism of irreversible protein denaturation. Biophys Chem 69:125–135
20. Burstein EA, Vedenkina NS, Ivkova MN (1973) Fluorescence and the location of tryptophan residues in protein molecules. Photochem Photobiol 18:263–279
21. Erker W, H, bler R, Decker H (2004) Structure-based calculation of multi-donor multi-acceptor fluorescence resonance energy transfer in the 4×6-mer tarantula hemocyanin. Eur Biophys J 33:386–395
22. Stryer L (1978) Fluorescence energy transfer as a spectroscopic ruler. Annu Rev Biochem 47:819–846
23. Dolashka P, Genov N, Parvanova K, Voelter W, Geiger M, Stoeva S (1996) *Rapana thomasiana* grosse (Gastropoda) hemocyanin: spectroscopic studies of the structure and conformational stability of the native protein and its structural subunits. Biochem J 315:139–144
24. Idakieva K, Siddiqui NI, Parvanova K, Nikolov P, Gielens C (2006) Fluorescence properties and conformational stability of the β-hemocyanin of *Helix pomatia*. Biochim Biophys Acta 1764:807–814
25. Reshetnyak Y, Burstein E (2001) Decomposition of protein tryptophan fluorescence spectra into log-normal components. II. The statistical proof of discreteness of tryptophan classes in proteins. Biophys J 81:1710–1734

26. Reshetnyak Y, Koshevnik Y, Burstein, E (2001) Decomposition of protein tryptophan fluorescence spectra into log-normal components. III. Correlation between fluorescence and microenvironment parameters of individual tryptophan residues. Biophys J 81:1735–1758
27. Perbandt M, Guth, hrlein E, Rypniewski W, Idakieva K, Stoeva S, Voelter W, Genov N, Betzel Ch (2003) The structure of a functional unit from the wall of a gastropod hemocyanin offers a possible mechanism for cooperativity. Biochemistry 42:6341–6346
28. Leyton P, Lizama-Vergara PA, Campos-Vallette MM, Becker MI, Clavijo E, Cordova Reyes I, Vera M, Jerez CA (2005) Surface enhanced Raman spectrum of nanomeric molecular systems. J Chil Chem Soc 50:725–730
29. Eftink MR, Ghiron CA (1981) Fluorescence quenching studies with proteins. Anal Biochem 114:99–227
30. Genov N, Shopova M, Boteva R, Jori G, Ricchelli F (1982) Chemical, Photochemical and spectroscopic characterization of an alkaline proteinase from *Bacillus subtilis* variant DY. Biochem J 207:193–200
31. Georgieva D, Schwark D, Nikolov P, Idakieva K, Parvanova K, Dierks K, Genov N, Betzel Ch (2005) Conformational states of the *Rapana thomasiana* hemocyanin and its substructures studied by dynamic light scattering and time-resolved fluorescence spectroscopy. Biophys J 88:1276–1282
32. Idakieva K, Gielens C, Siddiqui NI, Doumanova L, Vaseva B, Kostov G, Shnyrov V (2007) Irreversible thermal denaturation of b-hemocyanin of *Helix pomatia* and its substructures studied by differential scanning calorimetry. Z. Naturforschung 62a:499–506
33. Sterner R, Vogl T, Hinz H-J, Penz F, Hoff R, F, ll R, Decker H (1995) Extreme thermostability of tarantula hemocyanin. FEBS Lett 364:9–12
34. Shnyrov V, Zhadan G, Akoev I (1984) Calorimetric measurements of the effect of 330-MHz radiofrequency radiation on human erythrocyte ghosts. Bioelectromagnetics 5:411–418
35. Shnyrov V, Mateo P (1993) Thermal transitions in the purple membrane from *Halobacterium halobium*. FEBS Lett 324:237–240
36. Shnyrov V, Zhadan G (2000) Irreversible thermal dependence of complex biological structures. Recent Res Devel Physical Chem 4:351–367
37. Lumry R, Eyring H (1954) Conformational changes of proteins. J Phys Chem 58:110–120
38. Gebauer W, Stoeva S, Voelter W, Dainese E, Salvato B, Beltramini M, Markl J (1999) Hemocyanin subunit organization of the gastropod *Rapana thomasiana*. Arch Biochem Biophys 372:128–134
39. Georgieva DN, Stoeva S, Ali AA, Abbasi A, Genov N, Voelter W (1998) Circular dichroism study of the hemocyanin thermostability. Spectrochimica Acta A 54:765–771